# Internal vs Fishhook Hairpin DNA: Unzipping Locations and Mechanisms in the α-Hemolysin Nanopore

Yun Ding, Aaron M. Fleming, Henry S. White,* and Cynthia J. Burrows*

Department of Chemistry, University of Utah, 315 South 1400 East, Salt Lake City, Utah 84112-0850, United States

S *Supporting Information*

ABSTRACT: Studies on the interaction of hairpin DNA with the α-hemolysin (α-HL) nanopore have determined hairpin unzipping kinetics, thermodynamics, and sequence-dependent DNA/protein interactions. Missing from these results is a systematic study comparing the unzipping process for fishhook (one-tail) vs internal (two-tail) hairpins when they are electrophoretically driven from the *cis* to the *trans* side of α-HL via a 30-mer single-stranded tail. In the current studies, fishhook hairpins showed long unzipping times with one deep blockage current level. In contrast, the internal hairpins demonstrated relatively fast unzipping and a characteristic pulse-like current pattern. These differences were further explored with respect to stem length and sequence context. Further, a series of internal hairpins with asymmetric tails were studied, for which it was determined that a second tail longer than 12 nucleotides results in internal hairpin unzipping behavior, while tail lengths of 6 nucleotides behaved like fishhook hairpins. Interestingly, these studies were able to resolve a current difference of ∼6% between hairpin DNA immobilized in the nanopore waiting to unzip vs the translocating unzipped DNA, with the latter showing a deeper current blockage level. This demonstration of different currents for immobilized and translocating DNA has not been described previously. These results were interpreted as fishhook hairpins unzipping inside the vestibule, while the internal hairpins unzip outside the vestibule of α-HL. Lastly, we used this knowledge to study the unzipping of a long double-stranded DNA (>50 base pairs) outside the vestibule of α-HL. The conclusions drawn from these studies are anticipated to be beneficial in future application of nanopore analysis of nucleic acids.
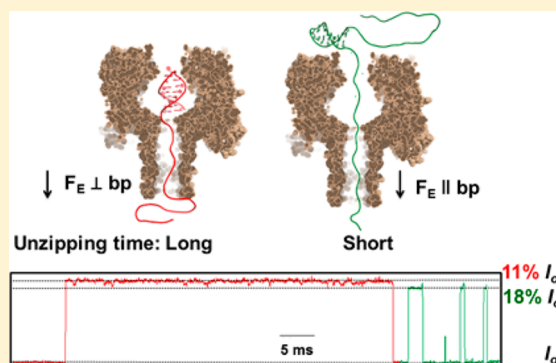
INTRODUCTION

Protein and solid-state nanopores have been utilized as sensors to detect DNA,[1−7] RNA,[1,6,8,9,4,10] and proteins.[11,12] In the past decade, the protein nanopore α-hemolysin (α-HL) has been well characterized and utilized as a sensor for biomolecules and a platform for label-free DNA sequencing.[13,7,14−17] Furthermore, α-HL has been employed to study the kinetics of DNA base pair unzipping for hairpin (intramolecularly base-paired)[18−25] and duplex (intermolecularly base-paired)[26−31] structures under an applied voltage. Various techniques, including magnetic and optical tweezers[32−35] and atomic force microscopy (AFM),[36,37] have been utilized to determine the force required to unzip DNA or RNA secondary structures. These systems, however, require end immobilization of the molecule. In contrast, the α-HL nanopore provides a label-free method to probe DNA molecules when electrophoretically driven through the channel. The capture of DNA molecules leads to a perturbation in the ion current through the α-HL nanopore that is readily detected.

The α-HL nanopore is composed of a wide vestibule and a narrow β-barrel.[15] The diameter of the β-barrel (1.4 nm)[15] allows translocation of single-stranded DNA or RNA (1 nm);[38] however, larger structures, such as hairpins and G-quadruplexes, have to unzip before they are driven through the nanopore by a voltage bias.[19,20,39−41] The current blockage level and the time it takes to unzip can provide information about the identity and the stability of the DNA or RNA secondary structures.[26,27,29] Recently, duplex unzipping through the α-HL ion channel has attracted much interest, and the unzipping kinetics and base pairing energy of duplex DNA have been extensively explored.[10,26−29,42−46]

Studies undertaken by Deamer, Akeson, and co-workers found that the interaction between terminal hairpins (without tails) and the α-HL nanopore led to a unique current modulation pattern when the hairpin interacted with the constriction zone on the *cis* side.[19−21,24] Later, fishhook hairpins (a terminal hairpin with one single-stranded tail) were used to study the kinetics and mechanism of hairpin unzipping in the α-HL nanopore.[22,47] More recently, the reverse (*trans* to *cis*) translocation dynamics of an internal hairpin (hairpin with two tails) was investigated by nanopore force spectroscopy.[34] Backward translocation (*trans* to *cis*) through the α-HL pore combined with theoretical modeling was considered as a promising approach for label-free single-molecule analysis of DNA and RNA folds.[34] The kinetics of

hairpin unzipping in the α-HL nanopore has been extensively studied, with an assumption that internal hairpins enter the vestibule of α-HL in the same fashion as a fishhook hairpin, i.e., with the base of the duplex region positioned on the lower floor of the protein vestibule and with one overhanging trail threaded into the narrow β-barrel.[34] Nevertheless, the location of hairpin unzipping remains unestablished for internal hairpins, and whether or not internal and fishhook hairpins unfold by the same mechanism in the nanopore experiment is not clear. Because internal DNA hairpins are a common secondary structure observed in single-stranded DNA, it is important to understand the behavior of these secondary structures and to explore the limits of nanopores for gaining information about nucleic acid structure and dynamics.

In the present work, an α-HL nanopore was constituted in a lipid bilayer suspended across the orifice of a glass nanopore membrane (GNM).[48] DNA oligomers were driven through the α-HL nanopore by an electrophoretic force from the *cis* to the *trans* side. The duration and current level while the oligomer blocked the nanopore correspond to the unzipping time and blockage current, respectively. We examined the effect of duplex stem length, sequence, and single-stranded tail length on the unzipping behaviors of a series of internal and fishhook hairpins. The unzipping characteristics of internal hairpins turned out to be very different from those of analogous fishhook hairpins, indicating they have different mechanisms of unzipping in the α-HL nanopore. Not only was the time of unzipping markedly affected by the unzipping mechanism, but the current levels observed during the two processes of denaturation were also distinctly different.

■ EXPERIMENTAL SECTION

Ion Channel Recording. A custom-built, high-impedance, low-noise amplifier and data acquisition system, designed and constructed by Electronic Biosciences (EBS), San Diego, CA, was used for the current−time (i−t) recordings. For all translocation studies, the DNA hairpin (2 nmol, 10 μM) was added and >1000 events were collected for each voltage with a 100 kHz low pass filter and a 500 kHz data acquisition rate. The composition of the buffered electrolyte solution was 1.00 M KCl, 10 mM PBS, and 1 mM EDTA (pH 7.4).

DNA Preparation and Purification Procedures. The oligodeoxynucleotides were synthesized from commercially available phosphoramidites (Glen Research, Sterling, VA) by the DNA-Peptide Core Facility at the University of Utah, followed by purification using a semipreparation ion-exchange HPLC column with a linear gradient of 30−100% B over 30 min while monitoring absorbance at 260 nm (B = 20 mM Tris, 1 M NaCl, pH 8 in 10% CH_3CN/90% ddH_2O; A = 10% CH_3CN/90% ddH_2O; flow rate = 3 mL/min). The purities of the oligodeoxynucleotides were determined by reinjecting the purified samples on an analytical ion-exchange HPLC running the previously mentioned buffers and method with the exception that the flow rate was 1 mL/min.

Ion Channel Measurements. The glass nanopore membrane (GNM; with radius 800 nm) was fabricated as previously reported.[49] 1,2-Diphytanoyl-*sn*-glycero-3-phospho-choline (DPhPC) bilayers spanning across the orifice of the GNM were prepared as previously described.[48] The protein α-HL was diluted to a 1 mg/mL solution in ultrapure water (18 MΩ·cm), and the DPhPC was dissolved in decane to a concentration of 10 mg/mL, both of which were stored at −80 °C. A pipet holder with a pressure gauge and a 10 mL gastight

syringe were used to attach the GNM to the DC system. Two Ag/AgCl electrodes were positioned inside and outside of the GNM to apply a voltage. A plastic pipet tip was used to paint the DPhPC solution (1 μL, 10 mg/mL) on the GNM surface. After addition of monomer α-HL (0.2 μL, 1 mg/mL), a pressure was applied to form a suspended bilayer, followed by reconstitution of a single α-HL nanopore in the bilayer. Populations of >1000 deep blockage events were collected for most of the experiments, and >500 deep blockage events were collected for those hairpins that took >0.5 s to unzip.

Data Analysis. Density plots were analyzed with software donated by EBS. Events were extracted using QUB 1.5.0.31 and fitted using Origin 8.5.1. Individual translocation i−t traces were refiltered to 2 or 10 kHz for presentation depending on the duration of single events. Due to the fact that different hairpins may have very different unzipping time and distributions, different numbers of bins (30−100) were used to fit the current or time histograms.

■ RESULTS AND DISCUSSION

As a preliminary study, one fishhook hairpin (F-hp12-1) and one internal hairpin (I-hp12-1) were designed to examine their behavior in the α-HL nanopore. (Note: F = fishhook; I = internal; 12 = base pairs (bp's) in the stem; the last number represents sequence variations studied; see Figure 1.) Both
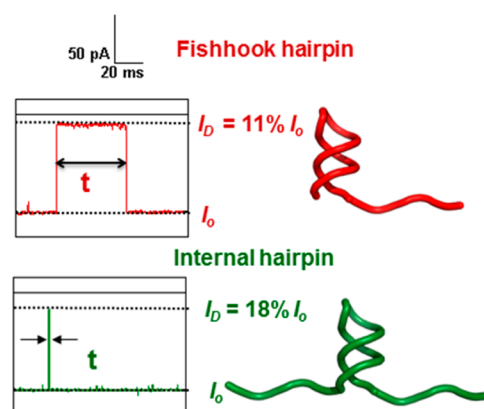
Figure 1. Typical fishhook (red) and internal (green) hairpin i−t traces observed at 100 mV bias (*trans* vs *cis*). The I_0 and I_D current levels are labeled. Cartoons for internal and fishhook hairpin structures are shown on the right. Sequence of the internal hairpin = 5′-C_{30} CGC GGC ATT AAA GTTA TTT AAT GCC GCG C_{30}-3′. Sequence of the fishhook hairpin = 5′-CGC GGC ATT AAA GTTA TTT AAT GCC GCG C_{30}-3′. Experimental conditions: 1.00 M KCl, 10 mM PBS, pH 7.4, 22.0 ± 0.5 °C.

hairpins have exactly the same loop, stem sequence, and tail length (Figure 1). According to Kasianowicz's work, a 30-mer poly-2′-deoxycytidine (dC_{30}) tail is sufficiently long to span the entire length of the α-HL channel.[50] Therefore, the internal hairpin was designed to have a dC_{30} tail at both the 3′ and 5′ ends, while the fishhook hairpin was designed to have only one dC_{30} tail at the 3′ end. Next, these two hairpins were subjected to identical conditions in the nanopore, while monitoring the time (t) and blockage current (I_D) during unzipping and translocation. According to a previous work, the current levels of events that are more blocking than 25% of the open channel current (I_0) are considered to be translocation events (I_D);[4] therefore, we only show and analyze deep blockage events in this work. The long events that are less blocking than 30% of I_0

were attributed to loop entry events where the loop of a hairpin enters the nanopore and cannot unzip; thus, they have to escape from the *cis* side of the channel. This observation was verified by experimentation on a dumbbell hairpin that can only enter via the loop, which leads to only long blocks with currents >30% I_o (Figures S1−S4, Supporting Information) similar to the ion currents observed with F-hp12-1 and I-hp12-1.

First, the durations of the unzipping/translocation events for the fishhook and internal hairpins were dramatically different (Figure 1). The distributions of unzipping times for F-hp12-1 and I-hp12-1 were well fit to an exponential decay function (Figures S1 and S4, Supporting Information) with a mean time constant (τ) that is reported for each hairpin's unzipping time, and the reported errors were determined from the fitting function errors. The fishhook hairpin required 64 ± 2 ms to unzip and translocate the pore, while the internal hairpins took 2.6 ± 0.1 ms under the conditions studied (1.00 M KCl and 100 mV bias). In other words, the duration for the internal hairpin unzipping and translocation was ∼20 times shorter than that for the fishhook hairpin. Second, the blockage current I_D was different between the internal and fishhook hairpins. The deep blockage current I_D for the internal hairpin was 18 ± 1% of I_o, while the I_D for the fishhook hairpin was 11 ± 1% of I_o. Considering these two hairpins have identical stem and loop sequences, it is remarkable that their unzipping times and blockage currents were so different.

To further support these results, the internal and fishhook hairpins were mixed together and unzipped using the same α-HL nanopore. These experiments confirmed that the fishhook hairpin was ∼6% more blocking than an internal hairpin in the same protein channel (Figure 2). Consistent with our previous results, it took at least 20 times longer (64 ± 2 ms vs 2.6 ± 0.1 ms) to unzip the fishhook hairpin than the internal hairpin (Figures 1 and 2). In addition, there are two peaks in the current plot for unzipping the internal hairpin, in which one was 17 ± 1% of I_o and the other was 19 ± 1% of I_o; this observation is consistent with the ability of this hairpin to unzip from either the 5′ or 3′ side depending upon the initial terminus captured and threaded into the nanopore.[51] Under the same conditions, the fishhook hairpin gave a single blocking current of 11 ± 1% of I_o, consistent with only 3′ entry. The fact that the I_D of the fishhook hairpin, which must enter from the 3′ terminus, does not match with either of the I_D levels for the internal hairpin is additional evidence that these two hairpins unravel by different mechanisms. The other key difference between these hairpins was observed in the current distributions; the fishhook hairpin displayed a narrow distribution in current blockage levels (Figure 2A and C), while the current distributions observed for the internal hairpin were broader (Figure 2B and C). Specifically, for the internal hairpins, the short duration events were more blocking than the longer duration events, leading to a tail toward the more blocking side (Figure 2B and C). Given that these two hairpins have exactly the same stem and loop, and the fact that they produced different blockage currents and unzipping times, suggests they unzip by different mechanisms.

When the unzipping events for the internal hairpins were examined more closely, two deep ion current blockage levels, I_A and I_B, were identified (Figure 3A). For the internal hairpins, the deep blockage current levels measured for I_A and I_B were 18 ± 1 and 13 ± 1% of I_o, respectively (Figure 3A). A single unzipping event began with a deep blockage I_{B1}, with a duration of 10 ± 5 μs, followed by a shallower blockage, I_A, with a
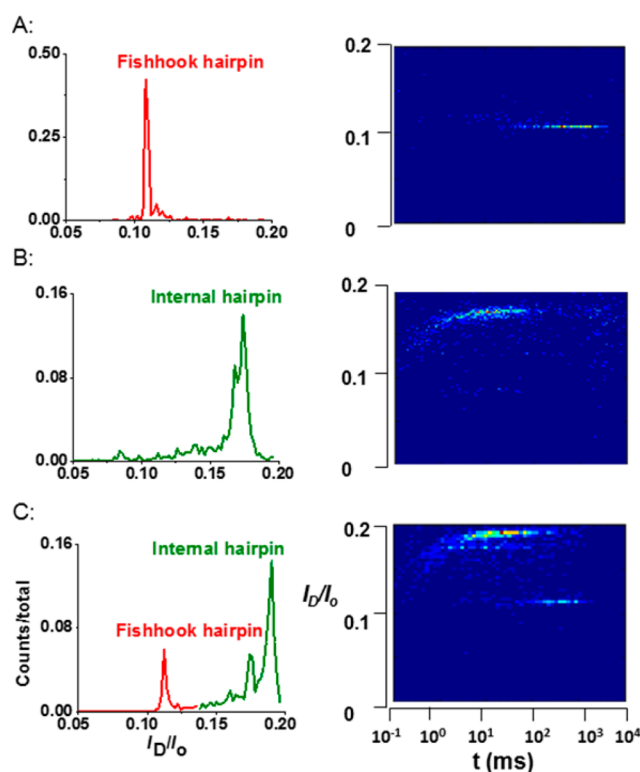
Figure 2. Current and time plots for unzipping experiments with internal and fishhook hairpins at 80 mV (*trans* vs *cis*). The left column is the current histogram showing the ratio of I_D/I_o. The right column shows scatter plots of I_D/I_o vs t. (A) Unzipping of fishhook hairpin alone; (B) unzipping of internal hairpin alone; (C) unzipping of both fishhook and internal hairpins using the same protein nanopore. Experimental conditions: 1.00 M KCl, 10 mM PBS, pH 7.4, 22.0 ± 0.5 °C. The data were binned differently for presentation purposes.

duration of 37 ± 2 ms, and ended with another deep blockage, I_{B2}, that had a duration of 150 ± 30 μs at 80 mV (*trans* vs *cis*). This current pulse pattern $I_o \rightarrow I_{B1} \rightarrow I_A \rightarrow I_{B2} \rightarrow I_o$ was observed in 50 ± 10% of the total events recorded. The only deviation from this pattern was a loss of the I_{B1} pulse in the remaining events (i.e., a $I_o \rightarrow I_A \rightarrow I_{B2} \rightarrow I_o$ pulse pattern), presumably because it was too short to be detected with the 100 kHz low-pass filter used in these studies (Figure 3A). A voltage-dependent study for internal hairpin unzipping was conducted on the internal hairpin (Figure 3B). The unzipping time distributions observed for the internal hairpins all gave a single exponential decay curve with a mean time constant, τ, that decreased as the voltage was increased (Figure S5, Supporting Information). The exponential time distribution signifies that a first-order process is occurring during unzipping; in previous studies, the kinetic process was proposed to be unzipping of the DNA secondary structure (i.e., hairpin or duplex).[52] In contrast to the data obtained for the internal hairpin, only one deep blockage current level (I_D) was identified for the fishhook hairpins (11 ± 1%, Figures 1 and 2A). This observation is consistent with previous literature reports.[22] The unzipping time constant for the fishhook hairpins decreased with increased voltage (Figure S6, Supporting Information). In conclusion, these data identify two key parameters that differ between the internal and fishhook hairpins: the unzipping time and the current blockage pattern.
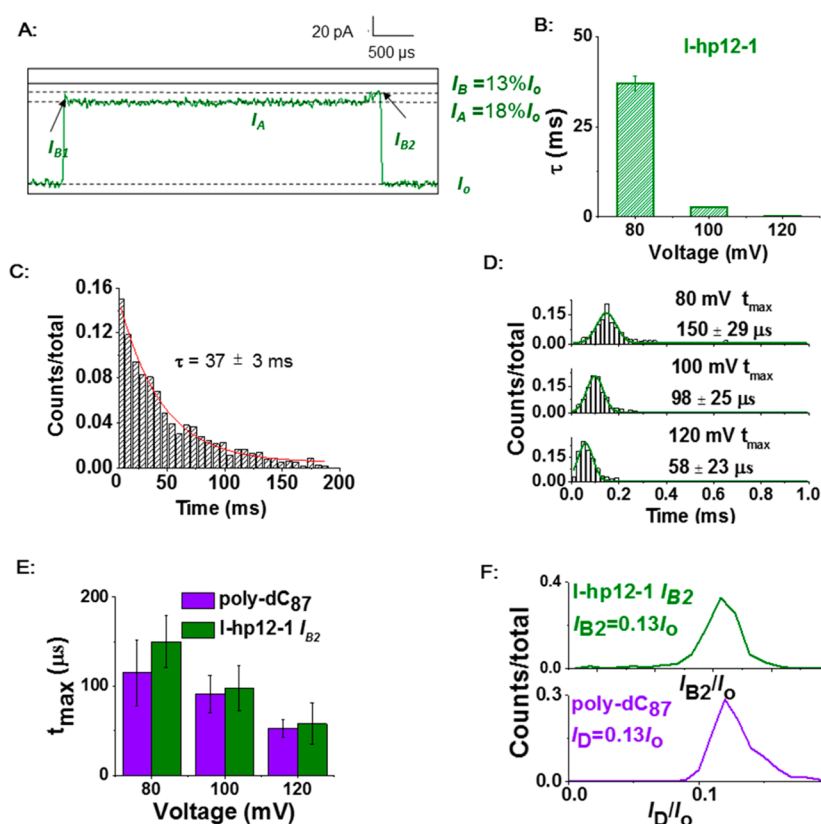
Figure 3. Unzipping and translocation of the internal hairpin. (A) A representative $i-t$ trace for unzipping the internal hairpin I-hp12-1 at 100 mV (*trans* vs *cis*). (B) Voltage-dependent unzipping time constant τ for I-hp12-1. (C) Histogram of unzipping time for the entire event and exponential decay fitting (red line) for I-hp12-1 at 80 mV (*trans* vs *cis*). (D) Voltage-dependent time histograms and Gaussian fits (green curve) for only the I_{B2} portion of I-hp12-1 events. (E) Comparison of the voltage-dependent t_{max} (peak values from Gaussian distributions) for dC_{87} (purple) and I_{B2} of I-hp12-1 (green). (F) Blocking current distribution for I_{B2}/I_o and I_D/I_o for I-hp12-1 (green) and dC_{87} (purple), respectively. Experimental conditions: 1.00 M KCl, 10 mM PBS, pH 7.4, 22.0 ± 0.5 °C.

Next, the blocking current pattern was studied more closely to determine the significance of each current level. It was established that the internal hairpin unfolded and translocated in the studies above; therefore, the following model is proposed to describe the $I_o \rightarrow I_{B1} \rightarrow I_A \rightarrow I_{B2} \rightarrow I_o$ current pattern. Given that the initial current changed from $I_o \rightarrow I_{B1}$, this identifies I_{B1} as the current associated with initial threading of the dC_{30} tail into the nanopore channel. Consistent with this hypothesis is the similarity in the I_{B1} current ($I_{B1} = I_{B2} = 13 \pm 1\%\ I_o$) with the blocking current observed for free translocation of a long homopolymer of dC that has a blocking current of 12 ± 2% under the same experimental conditions.[4] To support this claim, a control experiment was conducted in which a dC_{87} strand was allowed to translocate while monitoring the current and time (Figure 3E and F). In this control experiment, the same blocking current was observed for dC_{87} as monitored for I_{B1} of the internal hairpins unzipping, thus supporting our claim. The next current identified during the unzipping process of the internal hairpin was $I_{B1} \rightarrow I_A$, with I_A having a higher residual current (18 ± 1% I_o). We hypothesize this current corresponds to the stalling of the internal hairpin outside the vestibule of α-HL with one dC_{30} tail extending through the protein channel. Support for this claim comes from previous reports that monitored the current of poly dC strands when they were immobilized in the nanopore by a biotin–streptavidin complex. In these studies, the residual current of poly dC was ∼16% of I_o, which is higher than observed for free translocation of poly dC (∼13% I_o, Figure 3F).[51,53] Consistent

with stalling of the hairpin in the channel, I_A gives a larger residual current supporting the immobilization-like state of the internal hairpin. Moreover, it seems unlikely that both the 3′ and 5′ termini of the internal hairpin would thread into the vestibule of α-HL during the same event. On the basis of our model, we hypothesize that the internal hairpins presented here remain outside of the vestibule during the unzipping process. Therefore, the last current pulse, I_{B2}, must be associated with the translocation of the unfolded DNA strand derived from the internal hairpin. To support this hypothesis, the previous control study with the dC_{87} strand (similar length as the internal hairpin) was compared to I_{B2}. This comparison demonstrated that I_{B2} and the poly dC strand gave the same ion current 13 ± 1% I_o under these analysis conditions (1.00 M KCl and 100 mV bias, Figure 3F), and they showed similar translocation times (Figure 3E). As a further demonstration to identify I_{B2} as the translocation of the unfolded hairpin, the mean event time vs voltage was plotted and compared to dC_{87} (Figure 3E). Comparison of these event times gave similar values, as expected, because of the similarity in their strand length, confirming that I_{B2} was the translocation of the unfolded hairpin. In addition, the duration of the I_{B2} pulses showed a Gaussian distribution similar to unimpeded translocation events, whereas the entire event duration (dominated by the much longer I_A component) displays an exponential distribution of τ. In summary, the internal hairpin gave a unique pulse-like pattern during the unzipping and translocation process that we identify as threading of the poly dC tail, followed by

unzipping of the hairpin outside the vestibule that leads to translocation of the entire strand through the protein channel; this pulse-like pattern was not observed for the fishhook hairpins.

Previous studies have proposed that fishhook hairpins are pulled into the vestibule by the electrophoretic force, and unzip in the confined context of the vestibule.[22] This model is characterized by a single blockage current and long unzipping time, due to spatial confinement of the hairpin during unzipping, while the β-barrel is occupied by the tail.[22] In contrast, the internal hairpin, as described above, gave a short unzipping time with a unique pulse-like pattern in the blockage current (Figure 3A), for which we propose that the unzipping process occurs outside the vestibule.

Stem Length Dependence Studies. To further investigate the unzipping of internal hairpins through an α-HL nanopore, a group of internal hairpins was designed with the same dC$_{30}$ tails and loop sequence, but the length of the hairpin stem was increased from 9 to 15 base pairs (bp's) in 3 bp increments (Figure 4A). All of these internal hairpins gave the
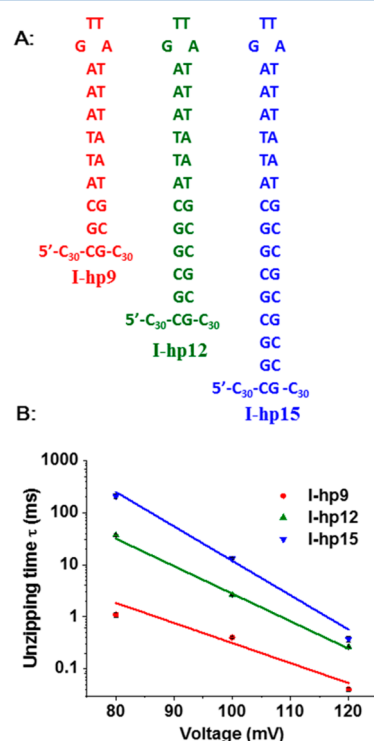

Figure 4. Unzipping time vs stem length for internal hairpins studied at different voltages (*trans* vs *cis*). (A) The sequences for the variable stem length internal hairpins. (B) Corresponding unzipping time vs applied bias. Experimental conditions: 1.00 M KCl, 10 mM PBS, pH 7.4, 22.0 ± 0.5 °C.

same pulse-like pattern to the blocking current, as described above. The measured unzipping time constant (τ) for these hairpins demonstrated that, as the stem length was increased, the unzipping time increased, as expected (Figure 4B). In these studies, τ showed an inverse correlation with voltage; this observation supports unzipping and translocation of the hairpins through α-HL (Figure S7, Supporting Information). Compared to the unzipping time of fishhook hairpins in the current work and those previously reported by Meller's laboratory,[22] the unzipping times of the internal hairpins were dramatically shorter, by a factor of ~20. Furthermore, the

unzipping times of variable stem length internal hairpins were sensitive to increased voltage that is consistent with a model of hairpin unzipping followed by translocation (Figure 4B).

Sequence Dependence Studies. Recently, Simmel and Gerland explored the sequence dependence of unfolding fishhook DNA hairpins by α-HL nanopores.[34] They reported that it took much longer to unzip a hairpin rich in G·C bp's compared to one rich in A·T bp's and hypothesized that the nature of the free energy landscapes for the unfolding process caused the observed differences because a G·C bp has one more hydrogen bond than an A·T bp.[25,34] Here we designed a group of fishhook hairpins with a 3′-dC$_{30}$ tail and an analogous group of internal hairpins to study the effect of sequence dependence on hairpin unzipping (Figure 5A). In each group, the hairpins
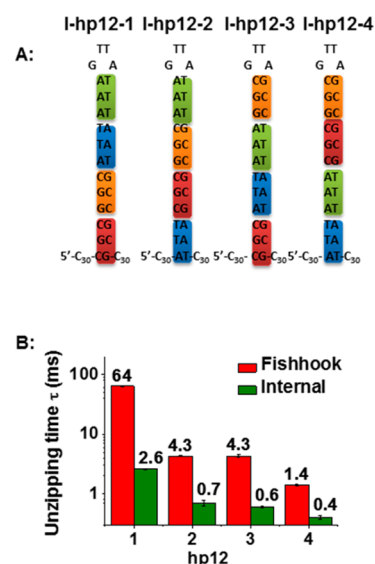
Figure 5. Dependence of unzipping time on stem sequence. (A) Sequence of internal hairpins from I-hp12-1 to I-hp12-4 that are comprised of four blocks of A·T or G·C bp's (color coded). (B) Unzipping times of internal and fishhook hairpins for hp1 to hp4 at 100 mV (*trans* vs *cis*). Fishhook hairpins lack the 5′-dC$_{30}$ tail shown for the internal hairpins. Experimental conditions: 1.00 M KCl, 10 mM PBS, pH 7.4, 22 ± 0.5 °C.

have the same tail, loop, and stem length (12 bp's), in which the variable studied was the sequence of base pairs in the stem. The sequences chosen for study were comprised of four different blocks of either three G·C or three A·T base pairs (Figure 5A). The nomenclature used for these hairpins has a number at the end to identify the sequence (i.e., I-hp12-1 = internal hairpin with a 12-bp stem comprised of sequence 1).

Unzipping experiments were performed on the various sequences of internal hairpins and fishhook hairpins. As shown in Figure 5B, internal hairpins and fishhook hairpins had dramatically different unzipping times even though they have exactly the same sequence in the hairpin stem. For the internal hairpin group, the experimental thermal melting values (T_m) were similar (Table SI 1, Supporting Information). Therefore, we expected similar unzipping times as recorded in our previous work.[27−29] In contrast to our expectation, it is demonstrated in Figure 5B that these internal hairpins have different unzipping time distributions (Figure S5, Supporting Information). For instance, I-hp12-1 is the most kinetically stable hairpin, requiring 37 ± 2 ms to unzip at 80 mV (*trans* vs *cis*), whereas it only took 0.7 ± 0.1 ms to unzip I-hp12-4 at the
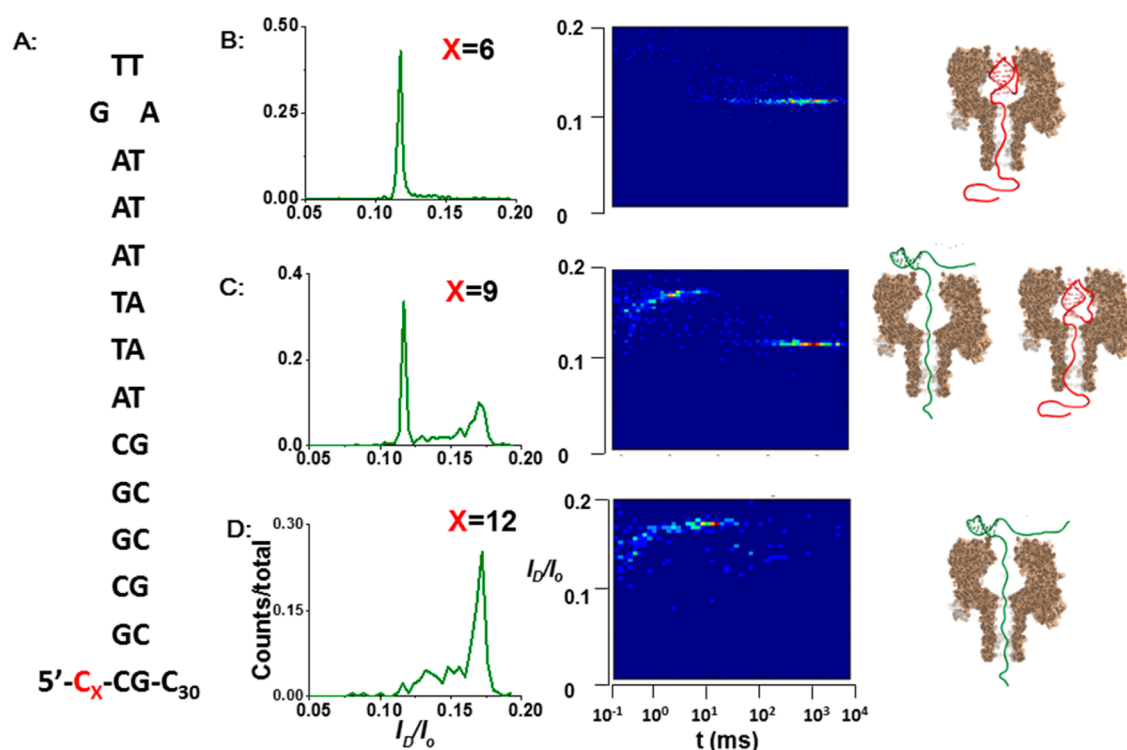
Figure 6. Unzipping current blockage and time of internal hairpins with asymmetric trails at 100 mV (*trans* vs *cis*). These three hairpins have the same 3′ tail, stem, and loop. The numbers of bases at the 5′ overhanging end are $X = 6$ (B), 9 (C), and 12 (D). The sequences of these hairpins are shown in part A. Experimental conditions: 1.00 M KCl, 10 mM PBS, pH 7.4, 22 ± 0.5 °C.

same bias, a factor of about 50 times faster than I-hp12-1. Surprisingly, the fishhook hairpin group showed a similar trend as that for the internal hairpin group, however, with much longer unzipping times (Figure 5B and Figure S8, Supporting Information). At 100 mV, fishhook F-hp12-4 was about 50 times faster to unravel than fishhook F-hp12-1. Additionally, the difference in blockage current patterns for the fishhook and internal hairpins remained the same in these studies. In short, there was a similar trend in terms of unzipping time in both hairpin groups; it took a much longer time to unzip the fishhook hairpins than the internal hairpins even though they have identical stem sequences.

The data collected in the sequence dependence study indicated that the location of the G·C and A·T bp blocks within the stem greatly affects the unzipping time of both internal and fishhook hairpins. The closer the G·C bp block was to the tail, the longer it took to unravel the hairpin. Once the unzipping process was initiated, it was easier to unzip the rest of the hairpin, even if it contained G·C-rich bp blocks. These data support the unzipping process being initiated from the end of the hairpin, because those with the more stable G·C blocks at the ends took longer to unzip than those with weaker A·T blocks at the ends (Figure 5B). This trend holds for both internal and fishhook hairpins.

Internal Hairpin with Asymmetric Tails Studies. The behavior of internal hairpins and fishhook hairpins is different in terms of unzipping current and time, which led us to the question, how many bases in the single-stranded tail are required to make the hairpin behave as an internal hairpin? The answer to this question will test our hypothesis that fishhook and internal hairpins unzip at different locations, leading to different unzipping mechanisms.

To address this question, a group of internal hairpins with asymmetric tails was designed. These hairpins have the same 3′ tail (dC_{30}), loop, and a 12-base-pair stem (Figure 6A). The 5′ end was systematically changed to include a 6-, 9-, or 12-mer dC tail. Experiments for these internal hairpins with asymmetric tails were conducted, and the unzipping currents and times were compared (Figure 6). These results show that the tail length is crucial to the behavior of the internal hairpins with asymmetric tails. When the 5′ tail was short (dC_6), it behaved like a fishhook hairpin (Figure 6B) with the blocking current (11% of I_o) being the same as F-hp12-1 and the unzipping time being even longer than that of F-hp12-1 (590 ± 50 ms vs 64 ± 2 ms at 100 mV). The longer unzipping time implies that the extra dC_6 tail increased the difficulty for the hairpin to unzip inside the vestibule. When the tail length was increased to 12 nucleotides (dC_{12}), it behaved like an internal hairpin (Figure 6D) with both the blocking current giving the pulse-like pattern described previously and the unzipping time being similar to that of an I-hp12-1 (3.7 ± 0.3 ms vs 2.6 ± 0.1 ms at 100 mV). Interestingly, when the 5′ tail was dC_9, two current peaks were observed, one was centered at 11% of I_o, similar to the fishhook hairpin F-hp12-1, and had a remarkably slow unzipping time (920 ± 60 ms at 100 mV, Figure 6C). The second population gave the pulse-like current pattern similar to I-hp12-1 with a similar unzipping time (3.0 ± 0.4 ms at 100 mV, Figure 5 and Figure S19, Supporting Information). The unzipping time for the asymmetric internal hairpin with the 9-mer tail further suggests that it behaved either as a fishhook or internal hairpin during unzipping depending on how it was captured by α-HL. These results demonstrate that a tail length of 12 nucleotides or greater causes the hairpin to exclusively unzip outside the vestibule of α-HL, tail lengths of 6 nucleotides or smaller unzip inside the vestibule, and tail lengths around 9 nucleotides

behave as both internal and fishhook hairpins with two distinct populations. Additionally, the internal hairpin with short, asymmetric tails had a significantly longer unzipping time than the fishhook hairpin, suggesting that the short tail can enter the vestibule of the α-HL and therefore hinder the unzipping process in the confined space of the protein cavity. This data further supports our hypothesis that the limited vestibule size causes slower unzipping for fishhook hairpins.

Unzipping a Long Hairpin with Asymmetric Tails. We have demonstrated that unzipping of internal hairpins and fishhook hairpins employs different mechanisms with the internal hairpins unzipping much faster than the fishhook hairpins. In a previous study from our laboratories, a 25-mer DNA duplex (similar to a fishhook hairpin that unzips in the vestibule) was not able to unzip and translocate under similar conditions (<140 mV in 1.00 M KCl);[28] therefore, we designed a long, internal hairpin with asymmetric tails to determine if we could unzip an internal hairpin with a long stem using the nanopore. This hairpin was designed to have 54 bp's in the stem, a 3′ dC_{12} tail, and a 5′ dC_{30} tail (Figure 7A). For this
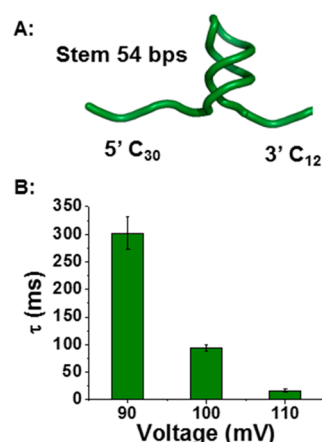
Figure 7. Unzipping of a long, asymmetric hairpin at 90, 100, and 110 mV (*trans* vs *cis*). (A) Cartoon of a long hairpin. (B) Voltage-dependent unzipping of a long, asymmetric hairpin (5′-C_{30} AGT TGC CAC CTA ATG CGT CGT CGG TCT ATC AAG CCT ACA CAG AAT CAG TTG TCG GTTA CGA CAA CTG ATT CTG TGT AGG CTT GAT AGA CCG ACG ACG CAT TAG GTG GCA ACT C_{12}-3′). Data were recorded at 80 mV, but the duration of unzipping was >2 s; therefore, a limited population of events were recorded that could not be used for proper statistical analysis to provide a time constant.

hairpin, we preferred to bias the system toward 5′ entry because it provides more information about chemical modification than the 3′ entry, based on our previous studies.[51]

As shown in Figure 7B, the unzipping time τ of this long hairpin displays strong voltage dependence and showed the characteristic pulse-like current pattern (Figure S15, Supporting Information) previously observed for internal hairpins. These observations indicate the unzipping and translocation of a long, internal hairpin with asymmetric tails can be rapid, supporting our hypothesis that internal hairpins unzip outside of the vestibule.

The data presented above support our hypothesis that internal hairpins and fishhook hairpins unzip at different locations before they can translocate through the α-HL nanopore, representing different unzipping mechanisms. Here, two possible explanations for these results are presented. In

previous studies, long duplex DNA or RNA unzipping was measured using optical tweezers and AFM, in which the force for dissociation was quantified. In these studies, the magnitude of the applied force was dependent on the orientation of the base pairs. A smaller force (10−30 pN), depending on the sequence,[33,35,54] was required to unfold or extend the structure when a parallel force was applied relative to the base pair axis, compared to the larger force being required when applied perpendicular to the base pair axis (65−300 pN).[36,54,55] Our results demonstrate that DNA molecules are easier to unwind when the unzipping electrophertic force, F_E, is applied parallel to the bp's; the unzipping times for internal hairpins in the α-HL nanopore are much shorter than those for the fishhook hairpins (Figure 3). In the process of unzipping of the fishhook hairpin, the electrophoretic force F_E is perpendicular to the bp's; therefore, it takes much longer to unzip and translocate these hairpins. Also, unlike internal hairpins, fishhook hairpins can enter the vestibule, and consequently, the unfolding occurs in this sterically demanding space; hence, fishhook hairpins have less freedom to change conformation to find the best state in which to unzip. However, for the internal hairpin remaining outside the protein nanopore, there is no space restriction, and it is much easier for it to find the conformation required to unzip.

CONCLUSIONS

In summary, the unzipping processes of internal and fishhook hairpins leading to translocation through the α-HL nanopore were explored. The data presented here show that, similar to the unzipping of fishhook hairpins, the unzipping of internal hairpins also depends on the stem length and stem sequence (Figures 4 and 5). More importantly, the data indicate that fishhook and internal hairpins unzip at different locations based on blockage current level patterns and the unzipping times recorded. Fishhook hairpins can enter the vestibule of α-HL and unzip in the spatially restricted context of the α-HL, leading to long unzipping times with one deep blockage current level. In contrast, the internal hairpins do not enter the vestibule and instead unzip outside the *cis* entrance of the α-HL channel, leading to fast unzipping times with a characteristic ion current pattern. This observation of slow unfolding inside the vestibule vs rapid unzipping outside the vestibule was also recently observed for G-quadruplexes of different folds,[41] some of which are small enough to enter the protein cavity, and others are too large and therefore unfold rapidly outside the vestibule under the influence of the applied electrophoretic force. On the basis of the data presented above, we propose that the location of unzipping leads to a different unzipping mechanism. In the case of the internal hairpin, the unzipping force is parallel to the base pair plane that renders that structure easier to unzip compared to the fishhook hairpin, in which the unzipping force is perpendicular to the base pair plane (Figure 8). Unzipping of the internal hairpins outside the vestibule gives a pulse-like pattern to the ion current that is characteristic of this process (Figure 3). The sequence-dependent studies support this hypothesis (Figure 5), because there was a 5−20-fold difference in unzipping times between fishhook hairpins and internal hairpins depending on the sequence and the applied voltage bias; additionally, the difference in ion current for the fishhook and internal hairpins remained the same for the sequences studied.

On the basis of our unzipping model for the hairpins, additional experiments were conducted to understand the

12879

dx.doi.org/10.1021/jp5101413 | J. Phys. Chem. B 2014, 118, 12873−12882
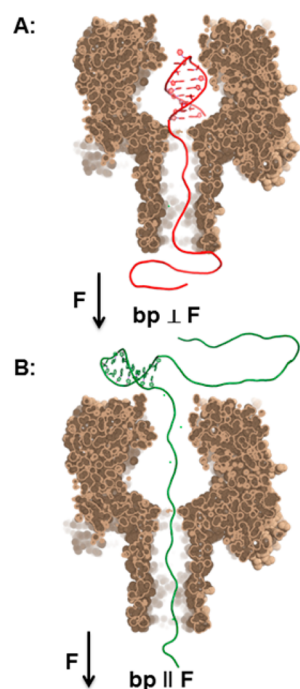
Figure 8. Relationship between the direction of the unzipping force and the base pairs in the hairpins studied. (A) The direction of unzipping force is perpendicular to the direction of the bp's, representing the unzipping of fishhook hairpins. (B) The direction of unzipping force is parallel to the direction of the bp's, representing the unzipping of internal hairpins. Structures were adapted from PDB 1AC7 and 7AHL.[56]

details of the unzipping process. First, a set of sequence-dependent studies suggest the position of C·G and A·T bp's contribute to the unzipping time of both fishhook and internal hairpins that is in agreement with experimental[25,34] and theoretical work.[57] Second, we identified that tail lengths ≥12 dC nucleotides transform fishhook hairpins to unzip like internal hairpins in the α-HL nanopore. Third, on the basis of our knowledge of the hairpin unzipping process, a long, internal hairpin (54-bp stem) with asymmetric tails was designed to determine if a long duplex (i.e., stem) could be unzipped outside the vestibule. These studies provide further insight into the process of DNA hairpin unwinding under an applied electrophoretic force and expand the possible avenues for analyzing DNA sequence and structure using protein nanopores such as α-hemolysin. Last but not least, these studies were able to resolve a current difference of ~6% between hairpin DNA immobilized in the nanopore waiting to unzip vs the translocating unzipped DNA, with the latter showing a deeper current blockage level. This demonstration of different currents for immobilized and translocating DNA has not been described previously.

ASSOCIATED CONTENT

Ⓢ Supporting Information

Fitting function, T_m data, hairpin sequence, sample $i-t$ traces, and event duration histograms. This material is available free of charge via the Internet at http://pubs.acs.org.

AUTHOR INFORMATION

Corresponding Authors

*Phone: (801) 585-6256. E-mail: white@chem.utah.edu.

*Phone: (801) 585-7290. E-mail: burrows@chem.utah.edu.

Notes

The authors declare no competing financial interest.

REFERENCES

(1) Wanunu, M. Nanopores: A journey towards DNA sequencing. *Phys. Life Rev.* **2012**, *9*, 125−158.

(2) Ashkenasy, N.; Sánchez-Quesada, J.; Bayley, H.; Ghadiri, M. R. Recognizing a single base in an individual DNA strand: a step toward DNA sequencing in nanopores. *Angew. Chem., Int. Ed.* **2005**, *44*, 1401−1404.

(3) Howorka, S.; Cheley, S.; Bayley, H. Sequence-specific detection of individual DNA strands using engineered nanopores. *Nat. Biotechnol.* **2001**, *19*, 636−639.

(4) Butler, T. Z.; Gundlach, J. H.; Troll, M. Ionic current blockades from DNA and RNA molecules in the alpha-hemolysin nanopore. *Biophys. J.* **2007**, *93*, 3229−3240.

(5) Zhao, Q.; Dimitrov, V.; Yemenicioglu, S.; Aksimentiev, A.; Timp, G. Stretching and unzipping nucleic acid hairpins using a synthetic nanopore. *Nucleic Acids Res.* **2008**, *36*, 1532−1541.

(6) Kasianowicz, J.; Brandin, E.; Deamer, D. Characterization of individual polynucleotide molecules using a membrane channel. *Proc. Natl. Acad. Sci. U.S.A.* **1996**, *93*, 13770−13773.

(7) Cherf, G. M.; Lieberman, K. R.; Rashid, H.; Lam, C. E.; Karplus, K.; Akeson, M. Automated forward and reverse ratcheting of DNA in a nanopore at 5-A precision. *Nat. Biotechnol.* **2012**, *30*, 344−348.

(8) Tian, K.; He, Z.; Wang, Y.; Chen, S.-J.; Gu, L.-Q. Designing a polycationic probe for simultaneous enrichment and detection of microRNAs in a nanopore. *ACS Nano* **2013**, *7*, 3962−3969.

(9) Shasha, C.; Henley, R. Y.; Stoloff, D. H.; Rynearson, K. D.; Hermann, T.; Wanunu, M. Nanopore-based conformational analysis of a viral RNA drug target. *ACS Nano* **2014**, *8*, 6425−6430.

(10) Wang, Y.; Zheng, D.; Tan, Q.; Wang, M. X.; Gu, L.-Q. Nanopore-based detection of circulating microRNAs in lung cancer patients. *Nat. Nanotechnol.* **2011**, *6*, 668−674.

(11) Rosen, C. B.; Rodriguez-Larrea, D.; Bayley, H. Single-molecule site-specific detection of protein phosphorylation with a nanopore. *Nat. Biotechnol.* **2014**, *32*, 179−181.

(12) Rodriguez-Larrea, D.; Bayley, H. Multistep protein unfolding during nanopore translocation. *Nat. Nanotechnol.* **2013**, *8*, 288−295.

(13) Cracknell, J. A.; Japrung, D.; Bayley, H. Translocating kilobase RNA through the staphylococcal α-hemolysin nanopore. *Nano Lett.* **2013**, *13*, 2500−2505.

(14) Boersma, A. J.; Bayley, H. Continuous stochastic detection of amino acid enantiomers with a protein nanopore. *Angew. Chem., Int. Ed.* **2012**, *51*, 9606−9609.

(15) Song, L.; Hobaugh, M.; Shustak, C.; Cheley, S.; Bayley, H.; Gouaux, J. Structure of staphylococcal alpha-hemolysin, a heptameric transmembrane pore. *Science* **1996**, *274*, 1859−1866.

(16) Manrao, E. A.; Derrington, I. M.; Laszlo, A. H.; Langford, K. W.; Hopper, M. K.; Gillgren, N.; Pavlenok, M.; Niederweis, M.; Gundlach, J. H. Reading DNA at single-nucleotide resolution with a mutant MspA nanopore and phi29 DNA polymerase. *Nat. Biotechnol.* **2012**, *30*, 349−353.

(17) Ayub, M.; Hardwick, S. W.; Luisi, B. F.; Bayley, H. Nanopore-based identification of individual nucleotides for direct RNA sequencing. *Nano Lett.* **2013**, *13*, 6144−6150.

(18) Dudko, O. K.; Mathé, J.; Szabo, A.; Meller, A.; Hummer, G. Extracting kinetics from single-molecule force spectroscopy: nanopore unzipping of DNA hairpins. *Biophys. J.* **2007**, *92*, 4188−4195.

(19) Vercoutere, W. A.; Winters-Hilt, S.; Olsen, H.; Deamer, D.; Haussler, D.; Akeson, M. Rapid discrimination among individual DNA hairpin molecules at single-nucleotide resolution using an ion channel. *Nat. Biotechnol.* **2001**, *19*, 248−252.

(20) Vercoutere, W. A.; Winters-Hilt, S.; DeGuzman, V. S.; Deamer, D.; Ridino, S. E.; Rodgers, J. T.; Olsen, H. E.; Marziali, A.; Akeson, M. Discrimination among individual Watson-Crick base pairs at the termini of single DNA hairpin molecules. *Nucleic Acids Res.* **2003**, *31*, 1311−1318.

(21) Winters-Hilt, S.; Vercoutere, W.; DeGuzman, V. S.; Deamer, D.; Akeson, M.; Haussler, D. Highly accurate classification of Watson-Crick basepairs on termini of single DNA molecules. *Biophys. J.* **2003**, *84*, 967−976.

(22) Mathé, J.; Visram, H.; Viasnoff, V.; Rabin, Y.; Meller, A. Nanopore unzipping of individual DNA hairpin molecules. *Biophys. J.* **2004**, *87*, 3205−3212.

(23) Mathé, J.; Aksimentiev, A.; Nelson, D. R.; Schulten, K.; Meller, A. Orientation discrimination of single-stranded DNA inside the α-hemolysin membrane channel. *Proc. Natl. Acad. Sci. U.S.A.* **2005**, *102*, 12377−12382.

(24) Deamer, D. W.; Vercoutere, W. A.; DeGuzman, V. S.; Lee, C. C. Sequence-dependent gating of an ion channel by DNA hairpin molecules. *Nucleic Acids Res.* **2006**, *34*, 6425−6437.

(25) Renner, S.; Bessonov, A.; Gerland, U.; Simmel, F. C. Sequence-dependent unfolding kinetics of DNA hairpins studied by nanopore force spectroscopy. *J. Phys.: Condens. Matter* **2010**, *22*, 454119−454119.

(26) Branton, D.; Sauer-Budge, A. F.; Nyamwanda, J. A.; Lubensky, D. K. Unzipping kinetics of double-stranded DNA in a nanopore. *Phys. Rev. Lett.* **2003**, *90*, 238101−238104.

(27) Jin, Q.; Fleming, A. M.; Burrows, C. J.; White, H. S. Unzipping kinetics of duplex DNA containing oxidized lesions in an alpha-hemolysin nanopore. *J. Am. Chem. Soc.* **2012**, *134*, 11006−11011.

(28) Schibel, A. E. P.; Fleming, A. M.; Jin, Q.; An, N.; Liu, J.; Blakemore, C. P.; White, H. S.; Burrows, C. J. Sequence-specific single-molecule analysis of 8-oxo-7,8-dihydroguanine lesions in DNA based on unzipping kinetics of complementary probes in ion channel recordings. *J. Am. Chem. Soc.* **2011**, *133*, 14778−14784.

(29) Jin, Q.; Fleming, A. M.; Ding, Y.; Burrows, C. J.; White, H. S. Structural destabilization of DNA duplexes containing single-base lesions investigated by nanopore measurements. *Biochemistry* **2013**, *52*, 7870−7877.

(30) Liu, A.; Zhao, Q.; Krishantha, D. M.; Guan, X. Unzipping of double-stranded DNA in engineered alpha-hemolysin pores. *J. Phys. Chem. Lett.* **2011**, *2*, 1372−1376.

(31) Wang, Y.; Tian, K.; Hunter, L. L.; Ritzo, B.; Gu, L. Q. Probing molecular pathways for DNA orientational trapping, unzipping and translocation in nanopores by using a tunable overhang sensor. *Nanoscale* **2014**, *6*, 11372−11379.

(32) Hyeon, C.; Thirumalai, D. Forced-unfolding and force-quench refolding of RNA hairpins. *Biophys. J.* **2006**, *90*, 3410−3427.

(33) Woodside, M. T.; Behnke-Parks, W. M.; Larizadeh, K.; Travers, K.; Herschlag, D.; Block, S. M. Nanomechanical measurements of the sequence-dependent folding landscapes of single nucleic acid hairpins. *Proc. Natl. Acad. Sci. U.S.A.* **2006**, *103*, 6190−6195.

(34) Schink, S.; Renner, S.; Alim, K.; Arnaut, V.; Simmel, F. C.; Gerland, U. Quantitative analysis of the nanopore translocation dynamics of simple structured polynucleotides. *Biophys. J.* **2012**, *102*, 85−95.

(35) Liphardt, J.; Onoa, B.; Smith, S. B.; Tinoco, I.; Bustamante, C. Reversible unfolding of single RNA molecules by mechanical force. *Science* **2001**, *292*, 733−737.

(36) Clausen-Schaumann, H.; Rief, M.; Tolksdorf, C.; Gaub, H. E. Mechanical stability of single DNA molecules. *Biophys. J.* **2000**, *78*, 1997−2007.

(37) Bustamante, C.; Smith, S. B.; Liphardt, J.; Smith, D. Single-molecule studies of DNA mechanics. *Curr. Opin. Struct. Biol.* **2000**, *10*, 279−285.

(38) Drew, H. R.; Wing, R. M.; Takano, T.; Broka, C.; Tanaka, S.; Itakura, K.; Dickerson, R. E. Structure of a B-DNA dodecamer: conformation and dynamics. *Proc. Natl. Acad. Sci. U.S.A.* **1981**, *78*, 2179−2183.

(39) An, N.; Fleming, A. M.; Burrows, C. J. Interactions of the human telomere sequence with the nanocavity of the α-hemolysin ion channel reveal structure-dependent electrical signatures for hybrid folds. *J. Am. Chem. Soc.* **2013**, *135*, 8562−8570.

(40) Shim, J. W.; Gu, L.-Q. Encapsulating a single G-quadruplex aptamer in a protein nanocavity. *J. Phys. Chem. B* **2008**, *112*, 8354−8360.

(41) An, N.; Fleming, A. M.; Middleton, E. G.; Burrows, C. J. Size-selective property of α-hemolysin provides signatures for DNA nanostructures formed by the human telomere sequence. *Proc. Natl. Acad. Sci. U.S.A.* **2014**, *111*, 14325−14331.

(42) McNally, B.; Wanunu, M.; Meller, A. Electromechanical unzipping of individual DNA molecules using synthetic sub-2 nm pores. *Nano Lett.* **2008**, *8*, 3418−3422.

(43) Sutherland, T. C.; Dinsmore, M. J.; Kraatz, H.-B.; Lee, J. S. An analysis of mismatched duplex DNA unzipping through a bacterial nanopore. *Biochem. Cell Biol.* **2004**, *82*, 407−412.

(44) Viasnoff, V.; Chiaruttini, N.; Bockelmann, U. Probing DNA base pairing energy profiles using a nanopore. *Eur. Biophys. J.* **2009**, *38*, 263−269.

(45) Zhang, X.; Wang, Y.; Fricke, B. L.; Gu, L.-Q. Programming nanopore ion flow for encoded multiplex microRNA detection. *ACS Nano* **2014**, *8*, 3444−3450.

(46) Johnson, R. P.; Fleming, A. M.; Jin, Q.; Burrows, C. J.; White, H. S. Temperature and electrolyte optimization of the α-hemolysin latch sensing zone for detection of base modification in double-stranded DNA. *Biophys. J.* **2014**, *107*, 924−931.

(47) Mathé, J.; Arinstein, A.; Rabin, Y.; Meller, A. Equilibrium and irreversible unzipping of DNA in a nanopore. *Europhys. Lett.* **2006**, *73*, 128−134.

(48) White, R. J.; Ervin, E. N.; Yang, T.; Chen, X.; Daniel, S.; Cremer, P. S.; White, H. S. Single ion-channel recordings using glass nanopore membranes. *J. Am. Chem. Soc.* **2007**, *129*, 11766−11775.

(49) Zhang, B.; Galusha, J.; Shiozawa, P. G.; Wang, G.; Bergren, A. J.; Jones, R. M.; White, R. J.; Ervin, E. N.; Cauley, C. C.; White, H. S. Bench-top method for fabricating glass-sealed nanodisk electrodes, glass nanopore electrodes, and glass nanopore membranes of controlled size. *Anal. Chem.* **2007**, *79*, 4778−4787.

(50) Henrickson, S. E.; DiMarzio, E. A.; Wang, Q.; Stanford, V. M.; Kasianowicz, J. J. Probing single nanometer-scale pores with polymeric molecular rulers. *J. Chem. Phys.* **2010**, *132*, 135101−135108.

(51) An, N.; Fleming, A. M.; White, H. S.; Burrows, C. J. Crown ether-electrolyte interactions permit nanopore detection of individual DNA abasic sites in single molecules. *Proc. Natl. Acad. Sci. U.S.A.* **2012**, *109*, 11504−11509.

(52) Maglia, G.; Heron, A. J.; Stoddart, D.; Japrung, D.; Bayley, H. Analysis of single nucleic acid molecules with protein nanopores. *Methods Enzymol.* **2010**, *475*, 591−623.

(53) Stoddart, D.; Heron, A. J.; Mikhailova, E.; Maglia, G.; Bayley, H. Single-nucleotide discrimination in immobilized DNA oligonucleotides with a biological nanopore. *Proc. Natl. Acad. Sci. U.S.A.* **2009**, *106*, 7702−7707.

(54) Rouzina, I.; Bloomfield, V. A. Force-induced melting of the DNA double helix 1. Thermodynamic analysis. *Biophys. J.* **2001**, *80*, 882−893.

(55) McCauley, M. J.; Williams, M. C. Mechanisms of DNA binding determined in optical tweezers experiments. *Biopolymers* **2007**, *85*, 154−168.

(56) van Dongen, M. J. P.; Mooren, M. M. W.; Willems, E. F. A.; van der Marel, G. A.; van Boom, J. H.; Wijmenga, S. S.; Hilbers, C. W. Structural features of the DNA hairpin d(ATCCTA-GTTA-TAGGAT): formation of a G-A base pair in the loop. *Nucleic Acids Res.* **1997**, *25*, 1537−1547.

(57) Krueger, A.; Protozanova, E.; Frank-Kamenetskii, M. D. Sequence-dependent basepair opening in DNA double helix. *Biophys. J.* **2006**, *90*, 3091−3099.